Rasha Hameed and Mohanned Al-Anber*

Department of Physics, College of Science, University of Basrah. Basrah, Iraq. rasha.hani@uobasrah.edu.iq, mohanned.mohammed@uobasrah.edu.iq

***Corresponding author:** mohanned.mohammed@uobasrah.edu.iq

Received: 14/02/2025. **Last Review:** 14/03/2025 **Accepted:** 05/06/2025

α-D-Glucose Adsorption on $Al_{24}N_{24}$ and Transition Metal-Doped $Al_{23}N_{24}$ Nanoclusters: New Insights for Biodetection

Abstract

This work examines the structural and electrical characteristics of pristine $Al_{24}N_{24}$ and X-doped $Al_{23}N_{24}$ nanoclusters (X = Co, Ni, or Si) in their interaction with α-D-glucose molecules. Utilizing B3LYP/6-311+G(d,p) computational methods, we examine the optimal geometries, binding energies, cohesive energies, and electrical properties of these nanoclusters. Our results indicate that $SiAl23N_{24}$ has the maximum binding energy, whereas $CoAl_{23}N_{24}$ presents just a marginal positive binding energy. The adsorption energies of glucose on these nanoclusters suggest a chemisorption mechanism. The study found that hexagonal $SiAl_{23}N_{24}$ and tetrahedral $NiAl_{23}N_{24}$ exhibited the most promising characteristics for glucose sensing due to significant bandgap changes, charge transfer, and high sensitivity. Additionally, octagonal $Al_{24}N_{24}$ showed potential as a ϕ-type glucose sensor.

Keywords: Nanoclusters; glucose adsorption; binding energy; density of states; biosensors.

Adsorción de α-D-glucosa en nanoclústeres de $Al_{24}N_{24}$ y $Al_{23}N_{24}$ dopados con metales de transición: nuevas perspectivas para la biodetección

Resumen

Este trabajo examina las características estructurales y eléctricas de nanoagrupaciones de $Al_{24}N_{24}$ virgen y $Al_{23}N_{24}$ dopado con X (X = Co, Ni o Si) en su interacción con moléculas de α-D-glucosa. Utilizando métodos computacionales B3LYP/6-311+G(d,p), examinamos las geometrías óptimas, las energías de enlace, las energías de cohesión y las propiedades eléctricas de estas nanoagrupaciones. Nuestros resultados indican que $SiAl_{23}N_{24}$ tiene la máxima energía de enlace, mientras que $CoAl_{23}N_{24}$ presenta solo una energía de enlace positiva marginal. Las energías de adsorción de glucosa en estas nanoagrupaciones sugieren un mecanismo de quimisorción. El estudio encontró que $SiAl_{23}N_{24}$ hexagonal y $NiAl_{23}N_{24}$ tetraédrico exhibieron las características más prometedoras para la detección de glucosa debido a cambios significativos de banda prohibida, transferencia de carga y alta sensibilidad. Además, $Al_{24}N_{24}$ octagonal mostró potencial como un sensor de glucosa de tipo ϕ.

Palabras clave: nanoclusters; adsorción de glucosa; energía de enlace; densidad de estados; biosensores.

Adsorção de α-D-glicose em nanoaglomerados de $Al_{24}N_{24}$ e $Al_{23}N_{24}$ dopados com metal de transição: novas perspectivas para a biodetecção

Resumo

Este trabalho examina as características estruturais e elétricas de nanoaglomerados virgens de $Al_{24}N_{24}$ e $Al_{23}N_{24}$ dopados com X (X = Co, Ni, Si) em relação à sua interação com moléculas de α-D-glicose. Utilizando métodos computacionais B3LYP/6-311+G(d,p), examinámos as geometrias ótimas, as energias de ligação, as energias coesivas e as propriedades elétricas destes nanoaglomerados. Os nossos resultados indicam que o $SiAl_{23}N_{24}$ apresenta a energia de ligação máxima, enquanto que o $CoAl_{23}N_{24}$ apresenta apenas uma energia de ligação positiva marginal. As energias de adsorção da glicose nestes nanoaglomerados sugerem um mecanismo de quimissorção. o estudo descobriu que o $SiAl_{23}N_{24}$ hexagonal e o $NiAl_{23}N_{24}$ tetraédrico exibiram as características mais promissoras para a deteção de glicose devido a alterações significativas no bandgap, transferência de carga e alta sensibilidade. Além disso, o $Al_{24}N_{24}$ octogonal apresentou potencial como sensor de glicose do tipo ϕ.

Palavras-chave: nanoclusters; adsorção de glicose; energia de ligação; densidade de estados; biossensores.

Introduction

The increase in diabetes prevalence and associated metabolic problems has heightened the necessity for efficient glucose monitoring devices. These systems are vital for regulating blood glucose levels and supplying critical information to avert issues related to diabetes. Conventional glucose monitoring methods, such as electrochemical sensors, have considerable limitations, including sensitivity, selectivity, and vulnerability to interference from other biomolecules. Consequently, there is an increasing interest in testing new materials and techniques to improve sensor efficacy.

Nanoclusters have emerged as particularly interesting options among these materials because of their distinctive electrical characteristics, elevated surface area, and capacity to promote improved interactions with glucose molecules [1]. Nanoclusters are defined as collections of atoms or molecules that exhibit unique electrical, optical, and chemical capabilities relative to their bulk equivalents. Recently, nanoclusters made of aluminium nitride (AlN) and its doped derivatives have attracted significant interest in biosensing applications. The capacity of these nanoclusters to establish stable complexes with biomolecules, along with their adjustable electrical properties, renders them outstanding candidates for glucose detection [2, 3]. The introduction of transition metal dopants, including cobalt (Co), nickel (Ni), and silicon (Si), into AlN nanoclusters can markedly modify their electrical structures and functional properties [4]. These adjustments increase the adsorption of energy and facilitate efficient charge transfer mechanisms, which are essential for enhancing sensor sensitivity and selectivity.

The adsorption of glucose onto nanoclusters is influenced by several parameters, including the geometric configuration of the nanocluster, the characteristics of the dopant, and the electrical interactions between the glucose molecule and the nanocluster surface. Prior research indicates that distinct adsorption configurations —namely, tetrahedral, hexagonal, and octagonal arrangements— result in differing contact strengths and electronic reactions [5]. Comprehending these arrangements and their related energetic properties is crucial for enhancing sensor design and efficacy. Theoretical simulations, especially those using density functional theory (DFT), offer significant insights into the adsorption energies and electrical characteristics of glucose-nanocluster complexes. These computational methods enable researchers to determine the optimal configurations for sensing applications, improving the design of next-generation glucose sensors [6].

The interaction between glucose and nanoclusters goes beyond simple physical adsorption; it includes intricate chemical interactions that can profoundly influence the electrical characteristics of the materials involved. For example, glucose may function as an electron donor, while the nanocluster surface could work as an electron acceptor. This interaction is essential for the design of efficient biosensors, as it directly influences the sensor's sensitivity and response time. Research has demonstrated that optimizing the orientation and position of the glucose molecules in relation to the nanocluster surfaces can enhance charge transfer efficiency [7]. This highlights the need to investigate multiple dopant combinations and structural topologies to improve the overall efficacy of glucose sensors.

Recent improvements in computational techniques have facilitated an extensive investigation of the interactions between glucose and nanoclusters, leading to novel sensor designs. The computation of Gibbs free energy changes (ΔG) throughout the adsorption process is essential, as it signifies the spontaneity and stability of the resultant complexes-critical criteria for sensor dependability [8]. Furthermore, examining the density of states (DOS) and variations in the highest occupied molecular orbital (HOMO) and lowest unoccupied molecular orbital (LUMO) energy gap (Eg) provides insights into the electrical properties of glucose-nanocluster systems. These findings clarify the mechanisms underlying electron transport and conductivity alterations following glucose adsorption [9]. Thermodynamic evaluations are essential for comprehending the energetics of the adsorption process. Configurations exhibiting lower ΔG values signify greater stability of adsorption complexes. This stability is essential in sensing applications, as it guarantees that the sensor can reliably respond to glucose levels without frequent recalibration or deterioration. Furthermore, the alterations in work function ($\Delta\phi$) due to glucose adsorption can offer insights into the sensor's efficacy.

A notable $\Delta\phi$ may signify a robust connection between the glucose molecule and the nanocluster surface, thereby increasing the sensor's sensitivity [10]. The electrical characteristics of glucose-nanocluster systems are similarly affected by the presence of dopants. Doping with transition metals can alter the electronic structure, resulting in variations in conductivity and reactivity. Research indicates that Ni doping in AlN nanoclusters increases their electron transfer efficiency and enhances their interaction with glucose molecules [11]. This improvement is due to the formation of localized states in the band structure, which promote charge transfer processes. Comprehending these alterations is essential for the development of sensitive glucose sensors.

Furthermore, the examination of the DOS and the Eg is crucial for evaluating the sensitivity of these systems. A reduced Eg often signifies that a molecule is more readily excited, indicating alterations in the system's conductivity. Studies demonstrate that glucose adsorption can substantially reduce the Eg, thus improving the sensor's sensitivity [12]. The correlation between electronic structure and sensor efficacy highlights the necessity of optimizing nanocluster architecture and dopant selection for efficient glucose detection. This investigation of glucose sensing by nanoclusters also includes the development of hybrid materials that integrate the benefits of nanostructures with alternative sensing methods. Integrating nanoclusters with optical sensors or using them with microfluidic systems could facilitate the development of multifunctional glucose monitoring platforms [13]. These developments may provide real-time monitoring of glucose levels with improved precision and faster reaction times.

This work examines the adsorption of α-D-glucose on both pristine and transition metal-doped AlN nanoclusters ($Al_{24}N_{24}$ and $Al_{23}N_{24}$) to determine the most advantageous configurations and evaluate their potential as glucose sensors. Furthermore, this study investigates the stability of different adsorption patterns and their influence on electrical properties to enhance the sensitivity and reliability of glucose detection systems. Our research will explain the complex interactions between glucose molecules and nanocluster surfaces, establishing a basis for future sensor development.

Materials and Methods

A popular exchange-correlation functional in DFT is the Becke Three-Parameter Hybrid Functional (B3), introduced by Becke in 1993. This functional, commonly referred to as B3LYP, integrates three components: Exact exchange energy from Hartree-Fock theory, exchange energy from a generalized gradient approximation, and correlation energy from methods such as the Lee-Yang-Parr (LYP) approach [14, 15]. B3LYP has proven to be effective for calculations involving III-V semiconductors [16]. The weak long-range interaction was corrected by adopting the empirical dispersion correction (DFT-D3(BJ)): Grimme's D3 correction with Becke-Johnson damping [17]. A popular basis set used is 6-311+G(d,p), which is a split-valence basis set enhanced with polarization functions, frequently applied in computational quantum chemistry [18–20]. Complete optimization was conducted using the B3LYP

functional with the 6-311+G(d,p) basis set, utilizing the Gaussian 09 program package (energy convergence = 10^{-6} a.u., force tolerance = 0.00045 a.u./Å) for all theoretical computations [21, 22]. Input files and output interpretation were managed using Gauss View 5.0 [23]. The DOS for all studied structures was plotted using the Gauss Sum 3.0 program [24]. The binding energy (E_{BE}) for the X (Co, Si, and Ni) doped $Al_{23}N_{24}$ nanocluster is defined in Eq. (1) [25]:

$$E_{BE} = E_{X\text{-nanocluster}} - (E_{nanocluster} + E_X) \quad (1)$$

Where $E_{X\text{-nanocluster}}$ and $E_{nanocluster}$ represent the total energies of the X-doped $Al_{23}N_{24}$ and $Al_{23}N_{24}$, respectively, and E_X denotes the energy of an isolated X atom.

To evaluate the sensing ability, the adsorption energy (E_{ads}) of the glucose molecule on the nanoclusters was calculated with Eq. (2):

$$E_{ads} = E_{Glucose + X\text{-nanocluster}} - (E_{X\text{-nanocluster}} + E_{Glucose}) \quad (2)$$

A negative E_{ads} indicates spontaneous adsorption, with more negative values suggesting greater stability [26–28]. If the absolute value of negative adsorption energy E_{ads} > 0.5 eV, the adsorption process can be judged as chemical adsorption; otherwise, it is physical adsorption [29, 30].

In this work, the adsorption behavior of glucose molecules on nanoclusters and X-doped nanoclusters was calculated at room temperature (298.15 K). Also, the band gap energy (Eg), the global hardness (η), and the electrophilicity index (ω) were calculated.

$$Eg = [E_{LUMO} - E_{HOMO}] \quad (3)$$

$$\eta = [E_{LUMO} - E_{HOMO}]/2 \quad (4)$$

$$\omega = [E_{LUMO} - E_{HOMO}]2/8\eta \quad (5)$$

Here, E_{LUMO} and E_{HOMO} refer to the lowest unoccupied molecular orbital and highest occupied molecular orbital, respectively [14, 15, 31]. Furthermore, we evaluated the sensitivity of the pristine and X-doped nanoclusters for glucose detection by calculating the percentage change in the band gap energy with Eq. (6):

$$\Delta Eg\% = [(Eg_2 - Eg_1)/Eg_1] \times 100\% \quad (6)$$

Where Eg_1 and Eg_2 are the Eg values before and after the adsorption of the glucose molecule, respectively. To investigate the interaction between the nanoclusters and glucose molecules, we calculated the Hirshfeld charge to determine the corresponding charge transfer (Q_{CT}) using the Eq. (7) [28]:

$$Q_{CT} = Q(\text{Glucose})_A - Q(\text{Glucose})_B \quad (7)$$

Where $Q(\text{Glucose})_A$ and $Q(\text{Glucose})_B$ represent the charge numbers of the target molecules after and before adsorption, respectively. A positive charge transfer ($Q_{CT} > 0$) indicates that electrons are transferred from the glucose molecule to the nanocluster, while a negative value suggests that electrons are transferred from nanoclusters to the glucose molecule.

Results and Discussion

Structure and geometry of pristine $Al_{24}N_{24}$, $CoAl_{23}N_{24}$, $NiAl_{23}N_{24}$, $SiAl_{23}N_{24}$ nanoclusters and α-D-glucose molecule

Figure 1 presents the optimized geometries of the pristine $Al_{24}N_{24}$, $CoAl_{23}N_{24}$, $NiAl_{23}N_{24}$, and $SiAl_{23}N_{24}$ nanoclusters, as well as the α-D-glucose molecule, using the B3LYP/6-311+G(d,p) method. Each nanocluster consists of twelve tetragons, eight hexagons, and six octagons, differing from the football shape of fullerene C60. Among these, $SiAl_{23}N_{24}$ exhibits the largest E_{BE} with the Si atom, accompanied by shorter bond lengths. In contrast, $CoAl_{23}N_{24}$ shows a slightly positive E_{BE}, while $NiAl_{23}N_{24}$ has a small negative E_{BE} with the $Al_{23}N_{24}$ nanocluster (refer to **figure 1**). Additionally, the aggregation potential of the X atom (where X = Co, Ni, or Si) within the X-$Al_{23}N_{24}$ nanocluster was investigated by calculating the cohesive energy (E_{coh}), using Eq. (8):

$$E_{coh} = (E_{X\text{-doped nanocluster}} - E_{iso\text{-}X})/N \quad (8)$$

Where $E_{iso\text{-}X}$ is the energy of a single atom and N is the number of atoms in the volume [32]. All four nanoclusters exhibit similar negative cohesive energies. Notably, $NiAl_{23}N_{24}$ and $SiAl_{23}N_{24}$ have EBE values exceeding the cohesive energy (E_{coh}) of their respective nanoclusters, indicating a relatively stable configuration. Overall, there are no significant differences in the cohesive energies of $CoAl_{23}N_{24}$, $NiAl_{23}N_{24}$, $SiAl_{23}N_{24}$, and the pristine $Al_{24}N_{24}$. The diffusion activation barrier (E_{act}) on the $Al_{23}N_{24}$ nanocluster characterizes the stability of Co, Ni, and Si-doped atoms. Machine learning calculations indicate that, for single atoms of various species, their energy barriers are proportional to E_{BE} and (E_{coh}). This relationship can be estimated using Eq. (9) [33]:

$$E_{act} = 0.637\,[E_{BE}^2/E_{coh}] - 0.203 \quad (9)$$

It is essential for E_{BE} to be higher than E_{coh} to prevent the formation of doping clusters within the nanocluster, as such clusters could diminish the ability to interact with other molecules by reducing the number of available adsorption sites. The trend observed for E_{act} is as follows: $SiAl_{23}N_{24}$ > $NiAl_{23}N_{24}$ > $CoAl_{23}N_{24}$, though the differences among these values are not significant. Additionally, all the doped

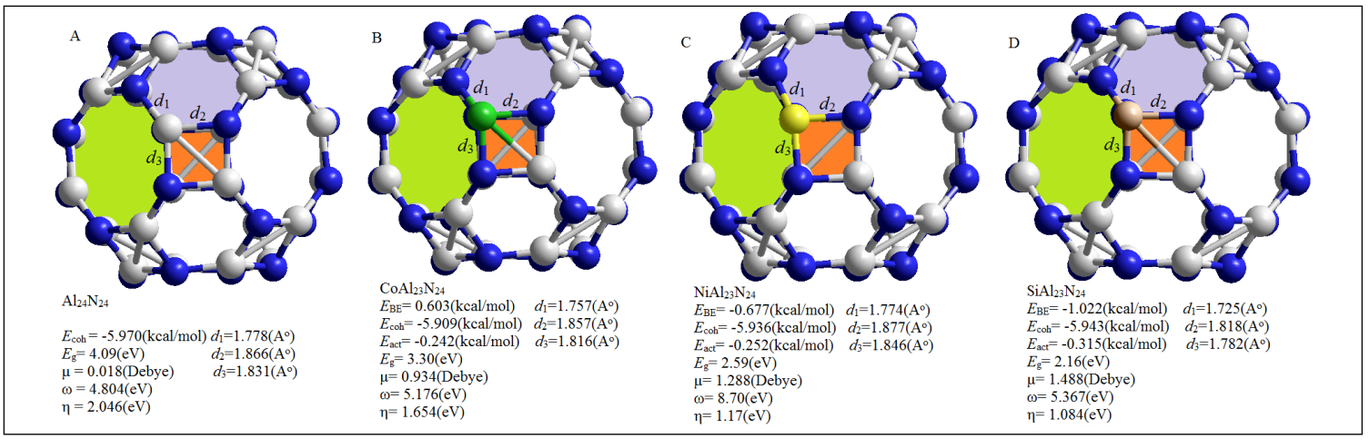

Figure 1. Geometrically optimized models. A: $Al_{24}N_{24}$, B: $CoAl_{23}N_{24}$, C: $NiAl_{23}N_{24}$, and D: $SiAl_{23}N_{24}$ nanocluster. These models were generated using the B3LYP/6-311+G(d,p) method. In the visualization, the colours represent different atoms: white for aluminium, blue for nitrogen, brown for silicon, green for cobalt, and yellow for nickel.

atoms exhibit binding energies equal to or smaller than 1 eV, indicating weak interactions between the doped atoms and the nanocluster [34]. In addition, substitutions can alter the electronic structure, including the band gap, where $Al_{24}N_{24}$, $CoAl_{23}N_{24}$, $NiAl_{23}N_{24}$, and $SiAl_{23}N_{24}$ have gotten 4.09, 3.30, 2.59, and 2.38 eV, respectively, which affects charge transfer and reactivity. Changes in the electronic properties can enhance or diminish stability depending on the specific interactions with surrounding molecules. Typically, $Al_{24}N_{24}$ exhibits uniform bond lengths due to its symmetrical structure. Due to silicon's different atomic size and electronegativity, the presence of silicon in $SiAl_{23}N_{24}$ may lead to shorter Si-N bond lengths than Al-N bonds in $Al_{24}N_{24}$. Transition metal binding (Co and Ni), in $CoAl_{23}N_{24}$ and $NiAl_{23}N_{24}$, often results in variable bond lengths due to *d*-orbital participation, which can cause slight elongation or contraction in Al-N bonds compared to $Al_{24}N_{24}$.

The α-D-glucose molecule adsorption on the pristine $Al_{24}N_{24}$ and X-$Al_{23}N_{24}$

Figure 2 presents the most favorable adsorption configurations of α-D-glucose on pristine $Al_{24}N_{24}$ and X-doped $Al_{23}N_{24}$ nanoclusters (where X = Co, Ni, and Si). The most stable complexes were identified from various initial configurations, with the glucose molecule positioned to have its surface parallel to the tetrahedral, hexagonal, and octagonal sides of the nanoclusters. The calculated adsorption energies (E_{ads}) for glucose on the nanoclusters show that the tetrahedral $NiAl_{23}N_{24}$, hexagonal $Al_{24}N_{24}$, tetrahedral $Al_{24}N_{24}$, and octagonal $NiAl_{23}N_{24}$ configurations yielded the highest values: −55.514, −44.441, −42.292, and −40.325 kcal/mol, respectively. These values indicate a chemisorption process.

Additionally, **figure 2** illustrates that glucose adsorption on octagonal $Al_{24}N_{24}$, octagonal $CoAl_{23}N_{24}$, hexagonal $Al_{24}N_{24}$, octagonal $SiAl_{23}N_{24}$, hexagonal $CoAl_{23}N_{24}$, and hexagonal $SiAl_{23}N_{24}$ substrates resulted in minimal deformation. The corresponding adsorption distances (charge transfer QCT) for these configurations are 1.995Å (−0.5091e), 1.990Å (−0.499e), 2.009Å (−0.483e), 2.055Å (−0.4513e), 2.007Å (−0.437e), and 2.080Å (0.3944e), respectively, indicating that glucose acts as an electron donor while the nanoclusters serve as electron acceptors. Furthermore, the thermodynamic parameters, specifically the Gibbs free energy (ΔG) for adsorbed glucose, were calculated.

As illustrated in **figure 2**, the negative ΔG values indicate spontaneous glucose adsorption. Notably, the tetrahedral $NiAl_{23}N_{24}$-glucose, hexagonal $Al_{24}N_{24}$-glucose, octagonal $CoAl_{23}N_{24}$-glucose, and hexagonal $SiAl_{23}N_{24}$-glucose configurations exhibit the highest spontaneous adsorption tendencies. This means that, under the given conditions, the system can move to the adsorbed state without additional energy.

Overall, tetrahedral $NiAl_{23}N_{24}$, hexagonal $Al_{24}N_{24}$, and tetrahedral $Al_{24}N_{24}$ got the highest negative ΔG values, which are crucial for understanding the energetics of adsorption and the stability of adsorbed complexes. They provide insights into the feasibility and efficiency of the interactions between α-D-glucose and the various nanocluster configurations. When α-D-glucose approaches the nanocluster, an initial interaction occurs due to electrostatic forces, van der Waals forces, or hydrogen bonding. This proximity is critical for electron transfer to take place.

The DOS at the Fermi level can indicate how readily electrons are transferred between glucose and the nanocluster. Higher resonance peaks in the DOS suggests stronger interactions. The DOS for the lowest-energy configuration of glucose on pristine $Al_{24}N_{24}$ is illustrated in **figure 3**. The DOS of glucose exhibits localized states, with resonance peaks observed between glucose and both hexagonal-$Al_{24}N_{24}$ and tetrahedral-$Al_{24}N_{24}$; however, these peaks diminish with octagonal-$Al_{24}N_{24}$.

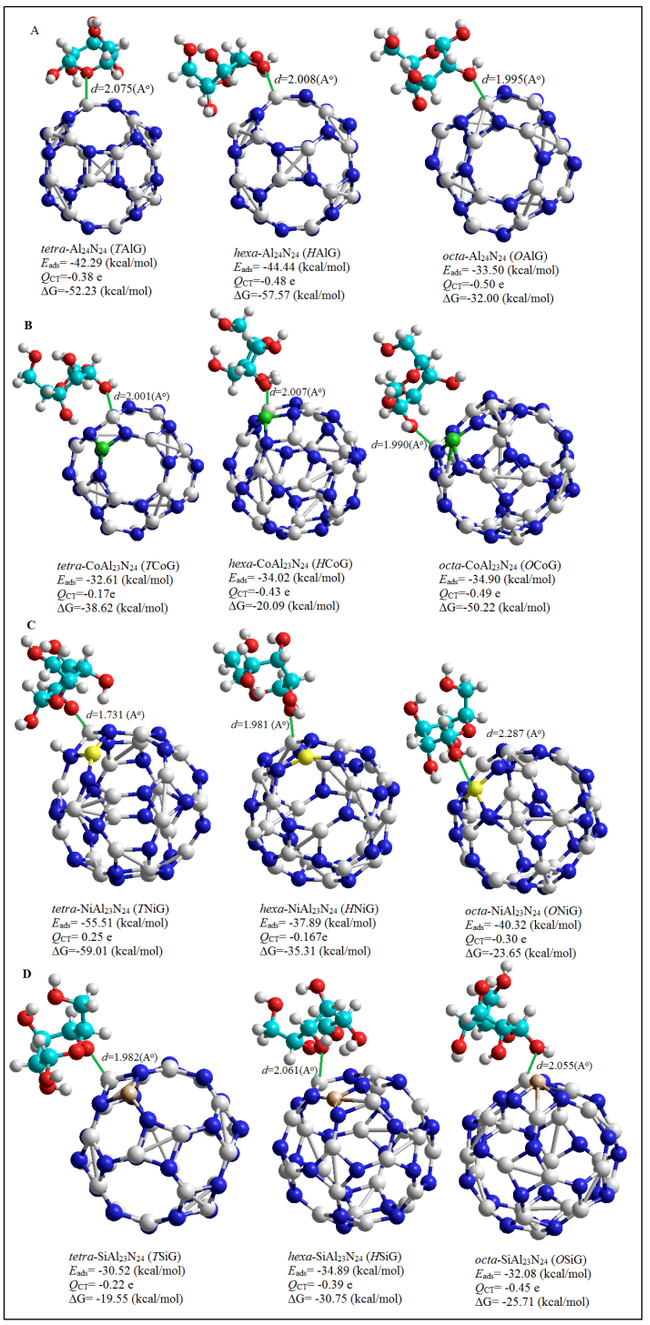

Figure 2. Geometrically optimized models. A: hexagonal-$Al_{24}N_{24}$-glucose, tetrahedral-$Al_{24}N_{24}$-glucose, octagonal-$Al_{24}N_{24}$-glucose; B: hexagonal-$CoAl_{23}N_{24}$-glucose, tetrahedral-$CoAl_{23}N_{24}$-glucose,octagonal-$CoAl_{23}N_{24}$-glucose;C:hexagonal-$NiAl_{23}N_{24}$-glucose, tetrahedral-$NiAl_{23}N_{24}$-glucose, octagonal-$NiAl_{23}N_{24}$-glucose; D: hexagonal-$SiAl_{23}N_{24}$-glucose, tetrahedral-$SiAl_{23}N_{24}$-glucose, and octagonal-$SiAl_{23}N_{24}$-glucose, respectively. These models were generated using the B3LYP/6-311+G(d,p) method. In the visualization, the colors represent different atoms: white for aluminium, grey for carbon, red for oxygen, white for hydrogen, blue for nitrogen, brown for silicon, green for cobalt, and yellow for nickel.

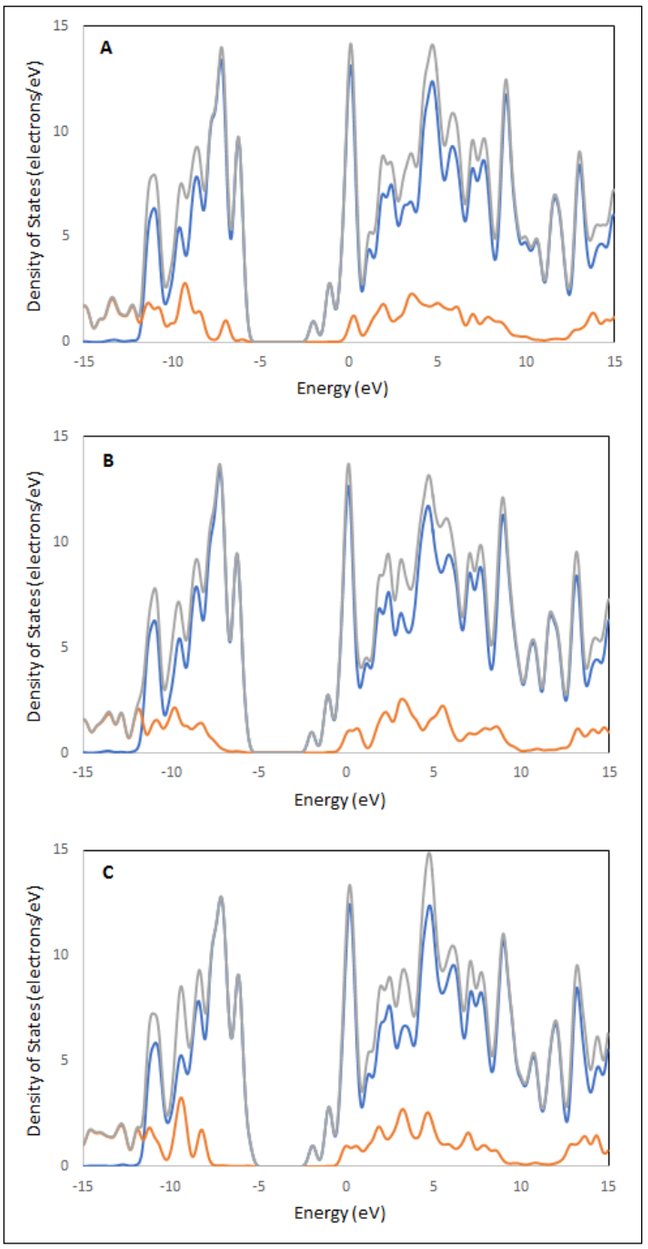

Figure 3. DOS of glucose and $Al_{24}N_{24}$ with A: tetrahedral-$Al_{24}N_{24}$-glucose, B: hexagonal-$Al_{24}N_{24}$-glucose, and C: octagonal-$Al_{24}N_{24}$-glucose. The orange, blue, and grey lines represent the levels of glucose, nanocluster, and glucose-nanocluster, respectively. The Fermi level is set to zero.

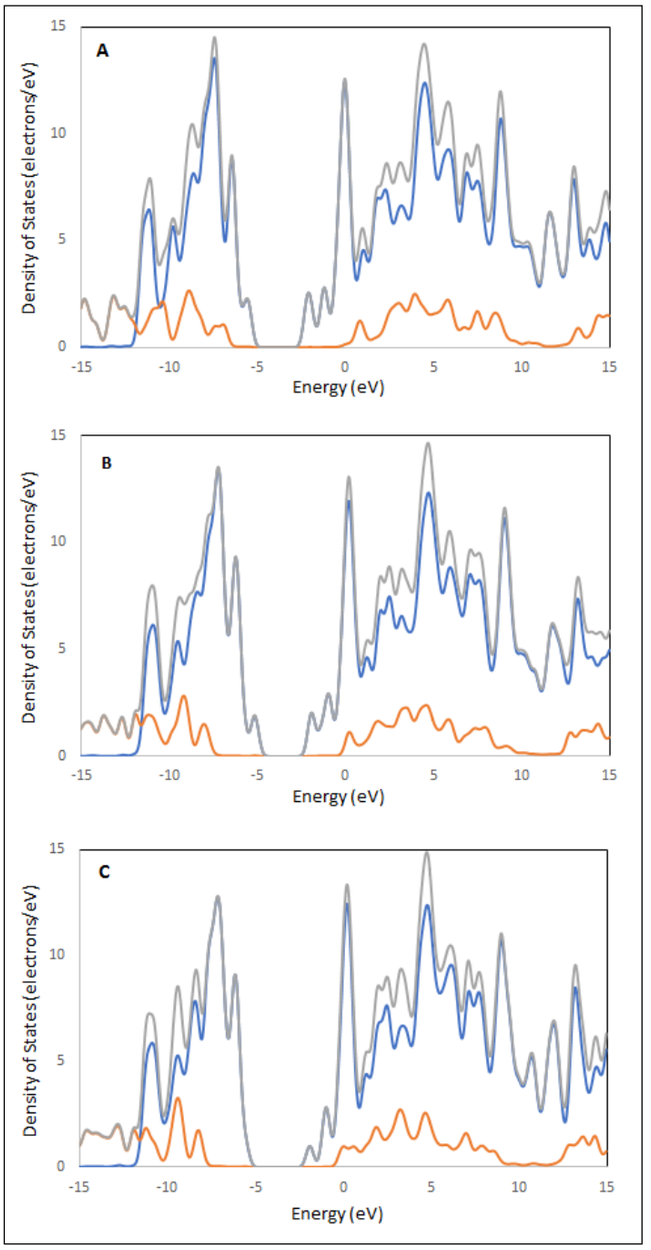

Figure 4. DOS of glucose and $CoAl_{23}N_{24}$ with A: tetrahedral-$CoAl_{23}N_{24}$-glucose, B: hexagonal-$CoAl_{23}N_{24}$-glucose, and C: octagonal-$CoAl_{23}N_{24}$-glucose. The orange, blue, and grey lines represent the levels of glucose, nanocluster, and glucose-nanocluster, respectively. The Fermi level is set to zero.

Figure 5A highlights a strong resonance peak between the glucose molecule and tetrahedral-$NiAl_{23}N_{24}$, indicating a significant interaction in the tetrahedral-$NiAl_{23}N_{24}$-glucose adsorption system. Conversely, the octagonal-$NiAl_{23}N_{24}$-glucose and hexagonal-$NiAl_{23}N_{24}$-glucose configurations exhibit reduced resonance, as shown in **figures 5B** and **5C**. In contrast, the $CoAl_{23}N_{24}$-glucose and $SiAl_{23}N_{24}$-glucose systems (**figures 4** and **6**) demonstrate only minimal interaction with glucose as compared to tetrahedral-$NiAl_{23}N_{24}$.

Generally, the type of dopant (e.g., Ni, Co, Si) affects electronic properties, influencing how the nanocluster interacts with glucose. For instance, Ni may enhance electron transfer and strengthen interactions. This suggests that the Ni-doped atom acts as an effective electron bridge, enhancing interactions between glucose and the adsorbent. Consequently, the $NiAl_{23}N_{24}$ nanocluster emerges as a promising candidate for glucose adsorption in biosensor applications.

These findings illustrate that the interactions between glucose and the four nanoclusters are not weak and mainly do not rely on van der Waals forces [35]. Thus, these nanoclusters are good bio-sensing materials for glucose due to their adsorption capacity. The orientation and position of the glucose molecule relative to the nanocluster (e.g., tetrahedral, octagonal, hexahedral arrangements) can lead to varying interaction strengths. Optimal alignment facilitates better overlap of electron orbitals. Overall, while all configurations perform well, $NiAl_{23}N_{24}$ and $Al_{24}N_{24}$ stand out as the most effective. A smaller gap indicates that the molecule can more easily undergo oxidation (donate electrons) or reduction (accept electrons).

The adsorption of glucose molecules on pristine tetrahedral-$Al_{24}N_{24}$ and hexagonal-$Al_{24}N_{24}$ had minimal impact on its electronic properties, as evidenced by the insignificant change in HOMO-LUMO gap (Eg) with the increasing rate (ΔEg) 2.7 and 5.8%, respectively, while octagonal-$Al_{24}N_{24}$ was increased (ΔEg = 10.5%), see **table 1**. This suggests that pristine octagonal-$Al_{24}N_{24}$ exhibits high sensitivity towards glucose adsorption and detection. Doped with Si, Co, and Ni atoms, however, significantly alter the electronic structure. The

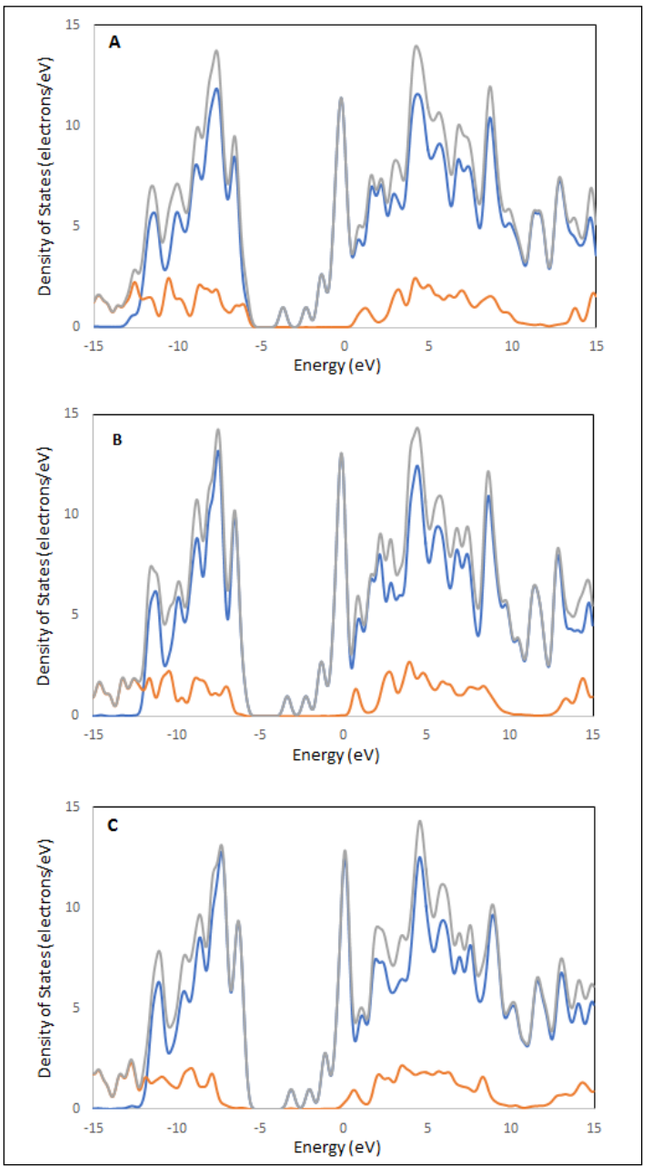

Figure 5. DOS of glucose and $NiAl_{23}N_{24}$ with A: tetrahedral-$NiAl_{23}N_{24}$-glucose, B: hexagonal-$NiAl_{23}N_{24}$-glucose, and C: octagonal-$NiAl_{23}N_{24}$-glucose. The orange, blue, and grey lines represent the levels of glucose, nanocluster, and glucose-nanocluster, respectively. The Fermi level is set to zero.

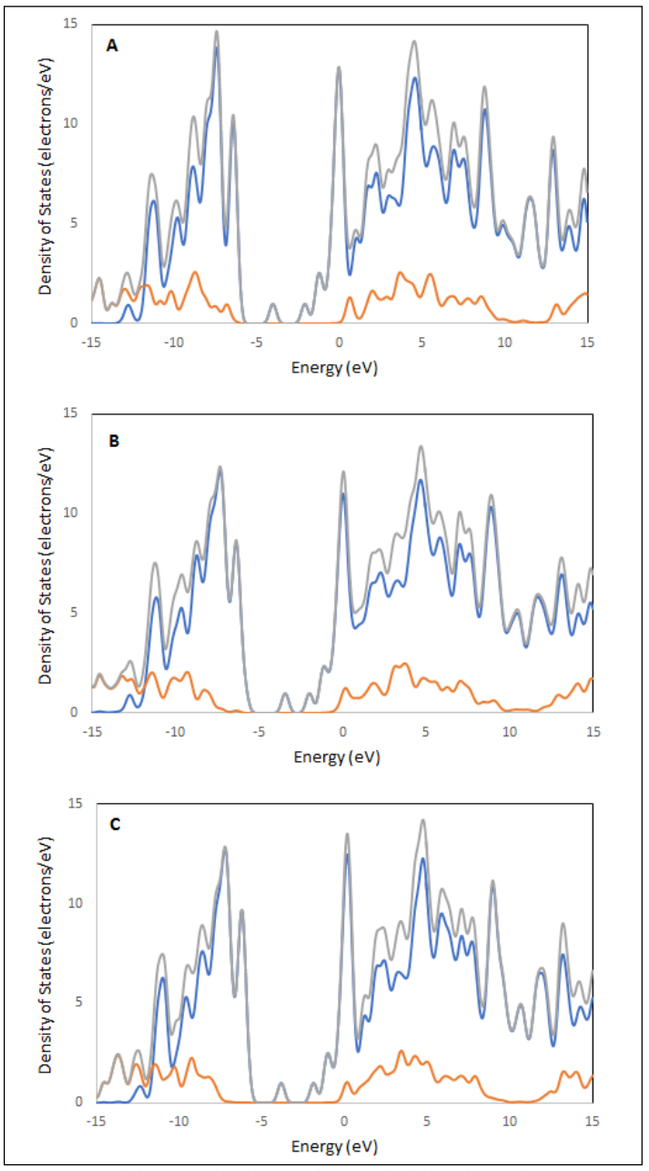

Figure 6. DOS of glucose and $SiAl_{23}N_{24}$ with A: tetrahedral-$SiAl_{23}N_{24}$-glucose, B: hexagonal-$SiAl_{23}N_{24}$-glucose, and C: octagonal-$SiAl_{23}N_{24}$-glucose. The orange, blue, and grey lines represent the levels of glucose, nanocluster, and glucose-nanocluster, respectively. The Fermi level is set to zero.

HOMO and LUMO levels undergo a substantial shift towards higher energies (**table 1**), leading to a concomitant narrowing of the *Eg*. These modifications potentially enhance the interaction between the X-doped $Al_{23}N_{24}$ and glucose molecules, suggesting an improved sensitivity for glucose detection, where tetrahedral-$SiAl_{23}N_{24}$, tetrahedral-$NiAl_{23}N_{24}$, and hexagonal-$SiAl_{23}N_{24}$ have insignificant change ratios in HOMO-LUMO gap (ΔEg) equal to 10.8, 15.7, and 32.4%, respectively. Generally, hexagonal-$SiAl_{23}N_{24}$ is favored.

The global hardness (η) of a material is defined as its intrinsic resistance to the transmission of electric charge. A positive correlation exists between a higher *Eg* value and reduced chemical reactivity, which leads to enhanced chemical stability. As shown in **figures 1** and **2**, η of Si, Co, and Ni-doped $Al_{23}N_{24}$ systems shows minimal variation before and after the presence of the glucose molecule. Notably, the highest difference ($\Delta\eta$ = 0.32) occurs in the hexagonal-$SiAl_{23}N_{24}$-glucose complex, followed by tetrahedral-$NiAl_{23}N_{24}$-glucose ($\Delta\eta$ = 0.20). In contrast, the electrophilicity index (ω) of these systems exhibits more significant fluctuations before and after glucose adsorption, particularly in the octagonal-$NiAl_{23}N_{24}$-glucose complex. These findings suggest that the $NiAl_{23}N_{24}$ nanocluster demonstrates a more pronounced affinity for the glucose molecule compared to the other adsorbents.

Analysis of the Sensing Mechanism

The preceding sections highlight the strong stability and adsorption capacity of tetrahedral-$NiAl_{23}N_{24}$, hexagonal-$Al_{24}N_{24}$, and tetrahedral-$Al_{24}N_{24}$ nanoclusters, making them suitable candidates for glucose sensing materials. In this section, we further analyze the sensitivity and desorption time of these nanoclusters to gain insight into the microscopic sensing mechanism. Generally, the *Eg* serves as an evaluation criterion for the excitability of a molecule; a smaller *Eg* typically indicates a molecule that is easier to excite, reflecting changes in the system's conductivity. According to **figure 3**, all nanoclusters exhibit a predominantly nonmetallic character, with the electronic *Eg* showing minimal variation after glucose adsorption, except for five specific nanoclusters. This suggests that the conductive behavior between the glucose molecule and these nonmetallic nanoclusters remains relatively stable, indicating poor glucose sensitivity. It is well-established that sensitivity can be assessed by examining the variation in electrical conductivity of the glucose-na-

Table 1. The energy Gap (*Eg*), energy gap change ratio (Δ*Eg*%), work function (Δϕ), global hardness (η), electrophilicity index (ω), electric dipole moment (μ), the desorption time (τ), and sensitivity (S).

Structure	*Eg*(eV)	Δ*Eg*%	Δϕ%	η (eV)	ω (eV)	μ (Debye)	τ (s)	S
tetrahedral-$Al_{24}N_{24}$-glucose	3.98	−2.72	−9.74	1.99	4.02	9.91	$6.34 \times 10^{+14}$	7.77
hexagonal-$Al_{24}N_{24}$-glucose	3.85	−5.80	−12.33	1.92	3.91	11.21	$2.33 \times 10^{+16}$	$1.018 \times 10^{+2}$
octagonal-$Al_{24}N_{24}$-glucose	3.66	−10.54	−16.30	1.83	3.76	15.62	$2.52 \times 10^{+8}$	$4.45 \times 10^{+3}$
tetrahedral-$SiAl_{23}N_{24}$-glucose	1.93	−10.85	−0.48	0.96	4.80	7.59	$1.69 \times 10^{+6}$	$9.64 \times 10^{+1}$
hexagonal-$SiAl_{23}N_{24}$-glucose	1.46	−32.47	−11.67	0.73	4.99	11.63	$2.60 \times 10^{+9}$	$8.87 \times 10^{+5}$
octagonal-$SiAl_{23}N_{24}$-glucose	1.95	−9.79	−6.95	0.97	4.14	13.85	$2.33 \times 10^{+7}$	$6.11 \times 10^{+1}$
tetrahedral-$CoAl_{23}N_{24}$-glucose	3.31	0.12	−7.44	1.65	4.42	7.56	$5.68 \times 10^{+7}$	1.71×10^{-1}
hexagonal-$CoAl_{23}N_{24}$-glucose	3.15	−4.64	−15.37	1.57	3.88	14.16	$6.08 \times 10^{+8}$	$3.81 \times 10^{+2}$
octagonal-$CoAl_{23}N_{24}$-glucose	3.23	−2.28	−13.41	1.61	3.97	14.85	$2.66 \times 10^{+9}$	$1.76 \times 10^{+1}$
tetrahedral-$NiAl_{23}N_{24}$-glucose	2.18	−15.8	−1.08	1.09	10.49	7.21	$2.70 \times 10^{+24}$	$7.47 \times 10^{+6}$
hexagonal-$NiAl_{23}N_{24}$-glucose	2.63	1.65	−3.68	1.31	8.24	6.08	$3.95 \times 10^{+11}$	4.27
octagonal-$NiAl_{23}N_{24}$-glucose	2.86	10.63	−5.29	1.43	7.32	8.01	$2.34 \times 10^{+13}$	$4.21 \times 10^{+4}$

nocluster adsorption system. The variation in sensitivity (S) can be calculated with Eq. (10) [36, 37]:

$$S = \exp[(Eg_2 - Eg_1)/k_BT] - 1 \quad (10)$$

In this equation, k_B is the Boltzmann constant (8.62×10^{-5} eV/K) and T is the working temperature of the molecular sensor. According to Eq. (10), sensor sensitivity is dependent on the variation of the *Eg* after glucose adsorption. Therefore, the hexagonal-$SiAl_{23}N_{24}$-glucose, tetrahedral-$NiAl_{23}N_{24}$-glucose, octagonal-$NiAl_{23}N_{24}$-glucose, and octagonal-$Al_{24}N_{24}$-glucose systems could exhibit high sensitivity as glucose sensors. Generally, if the energy gaps remain unchanged, it indicates minimal effects on the resistivity when glucose is adsorbed onto the nanoclusters, suggesting that the sensitivity of these nanoclusters to glucose molecules is poor.

The present study investigated the impact of glucose molecules on the Fermi levels (E_F) and the work function (ϕ), where $\phi = -E_F = [E_{LUMO} - E_{HOMO}]/2$ denotes the energy required to remove an electron from the Fermi level. The Δϕ measured by the Kelvin oscillator influences the gate voltage in the sensor. This variation generates an electrical signal that can be correlated with the concentration of the adsorbed glucose, facilitating quantitative analysis [38, 39]. The Δϕ resulting from the adsorption of a substance affects the gate voltage and generates an electrical signal that aids in recognizing the chemical [40, 41]. The Δϕ values for pristine and Co, Si, and Ni-doped nanoclusters after glucose adsorption are presented in **figure 3**. The Δϕ% values for the nanoclusters upon glucose adsorption are as follows:

−16.3% for octagonal-$Al_{24}N_{24}$-glucose

−15.3% for hexagonal-$CoAl_{23}N_{24}$-glucose

−13.4% for octagonal-$CoAl_{23}N_{24}$-glucose

−12.3% for hexagonal-$Al_{24}N_{24}$-glucose

−11.6% for hexagonal-$SiAl_{23}N_{24}$-glucose

These results indicate that the most significant Δϕ occurs in the octagonal-$Al_{24}N_{24}$ upon interaction with glucose, followed closely by the hexagonal-$CoAl_{23}N_{24}$ system. The ϕ serves as a valuable metric for assessing the effectiveness of the sensor. In summary, "octa" and "hexa" are crucial for understanding the structural characteristics and potential performance of nanoclusters in sensing applications.

The dipole moment, resulting from unequal charge distribution in nanostructures, is crucial for comprehending the interaction between glucose and $Al_{24}N_{24}$. We calculated dipole moments for both the adsorbent and substrate before and after contact (**figure 1**, **table 1**). A notable discovery is the substantial increase in dipole moment after glucose adsorption. The dipole moments of the glucose-nanocluster complexes produced were much more significant than those of the isolated glucose molecules or nanocages. This enhancement indicates a substantial alteration in the distribution of charges post-adsorption due to the charge exchange between the glucose molecule and the nanocage. The following dipole moments for the glucose-nanocluster complexes were documented:

15.62 D for octagonal-$Al_{24}N_{24}$-glucose

14.85 D for octagonal-$CoAl_{23}N_{24}$-glucose

14.16 D for hexagonal-$CoAl_{23}N_{24}$-glucose

13.85 D for hexagonal-$SiAl_{23}N_{24}$-glucose

11.63 D for hexagonal-$Al_{24}N_{24}$-glucose

These findings show that glucose and the $Al_{24}N_{24}$ nanocluster have a strong interaction that is mediated by charge transfer. The considerable rise in dipole moment upon glucose adsorption suggests that the interaction is not just happening on the surface but also involves a significant change in where the electrons are distributed. This charge transfer and the increased dipole moment that follows are probably crucial for the binding affinity that was seen and could be used for sensing purposes. It's also worth noting that the dipole moment changes between doped and undoped nanocluster structures, as well as between hexagonal and octagonal structures. This suggests that the composition and shape of the nanocluster can affect how strongly it interacts with glucose [42].

Furthermore, the desorption property (τ) is crucial for assessing the repeatability of a sensor. Moderate interactions between nanoclusters and molecules facilitate the desorption of the adsorbate in a short time, allowing for sustainable device utilization. Based on the transition state theory, we calculated thedesorption time (τ) using Eq. (11) [43]:

$$\tau = f_o^{-1} \exp[-E_{abs}/k_BT] \quad (11)$$

Where f_o is the attempt frequency, E_{abs} is the adsorption energy, k_B is the Boltzmann constant (8.62×10^{-5} eV/K), and T is the temperature. In this study, we adopted an attempt frequency value of 1×10^{-16} s^{-1}, as reported in the literature [44, 45]. The desorption times for glucose over the nanoclusters at the working temperature of 298 K are shown for hexagonal-$SiAl_{23}N_{24}$-glucose, octagonal-$SiAl_{23}N_{24}$-glucose, and tetrahedral-$NiAl_{23}N_{24}$-glucose, as illustrated in **figure 3**.

Conclusions

This study demonstrates how nanoclusters shape and doping collaboratively influence glucose sensing efficacy, providing design

principles for advanced sensors. These findings reveal that doping plays a critical role in determining sensing mechanisms. Ni-doped clusters exhibit strong chemisorption (−55.51 kcal/mol) due to Ni's high d-electron affinity, which facilitates charge transfer from glucose (Q_{CT} = 0.25e). This suggests that Ni sites act as electron sinks, making them well-suited for redox-based detection. In contrast, silicon-doped clusters demonstrate substantial bandgap modulation (−32.4%), which is attributed to silicon's capacity to disrupt the delocalized ϖ-electron networks within AlN frameworks, a property advantageous for electronic (*Eg*-type) sensors. Additionally, the work function change ($\Delta\phi$) in pristine $Al_{24}N_{24}$ (−16.3%) highlights the importance of surface dipole effects in field-effect transistor (FET) sensing platforms.

The study also establishes clear topology-property relationships: structural geometry impacts sensor performance. The hexagonal $SiAl_{23}N_{24}$ cluster exhibits exceptional sensitivity (8.87×10^5) due to its open framework, which enhances glucose accessibility to active silicon sites. Conversely, the compact tetrahedral structure of $NiAl_{23}N_{24}$ improves adsorption stability but restricts bandgap response, emphasizing the trade-offs between steric constraints and electronic effects. These insights underscore the necessity of balancing dopant-induced electronic modulation with geometric accessibility in sensor design.

For practical implementation, further research should assess potential interference from biomolecules such as fructose to validate clinical applicability. Additionally, the distinct work function variations in $Al_{24}N_{24}$ suggest its compatibility with FET-based platforms, while Ni-doped clusters may be better suited for electrochemical strips. Overall, this work identifies Ni/Si-doped AlN nanoclusters as promising candidates for glucose sensing and establishes a framework for optimizing doping strategies and nanostructure design in next-generation detectors.

Acknowledgments

The authors gratefully acknowledge the support provided by the Molecular Engineering and Computational Modeling Lab, Department of Physics, College of Science, University of Basrah, for facilitating the computational resources and research environment essential for this study.

References

[1] A. J. González Fá, V. Orazi, E. A. González, A. Juan, and I. López-Corral, "DFT study of β-D-glucose adsorption on single-walled carbon nanotubes decorated with platinum. A bonding analysis," *Appl. Surf. Sci.*, vol. 423, pp. 542–548, 2017. DOI: https://doi.org/10.1016/j.apsusc.2017.05.227.

[2] E. A. Eno *et al.*, "Molecular modeling of Cu-, Ag-, and Au-decorated aluminum nitride nanotubes for hydrogen storage application," *ACS Appl. Energy Mater.*, vol. 6, no. 8, pp. 4437–4452, 2023.

[3] F. Kamali, G. Ebrahimzadeh-Rajaei, S. Mohajeri, A. Shamel, and M. Khodadadi-Moghaddam, "A computational design of X24Y24 (X = B, Al, and Y = N, P) nanoclusters as effective drug carriers for metformin anticancer drug: A DFT insight," *Inorg. Chem. Commun.*, vol. 141, p. 109527, Jul. 2022. DOI: https://doi.org/10.1016/J.INOCHE.2022.109527.

[4] I. Benjamin *et al.*, "Transition metal-decorated B12N12–X (X= Au, Cu, Ni, Os, Pt, and Zn) nanoclusters as biosensors for carboplatin," *ACS omega*, vol. 8, no. 11, pp. 10006–10021, 2023.

[5] Q. He *et al.*, "Phase engineering and synchrotron-based study on two-dimensional energy nanomaterials," *Chem. Rev.*, vol. 123, no. 17, pp. 10750–10807, 2023.

[6] T. Saha *et al.*, "Wearable electrochemical glucose sensors in diabetes management: a comprehensive review," *Chem. Rev.*, vol. 123, no. 12, pp. 7854–7889, 2023.

[7] R. Jin, G. Li, S. Sharma, Y. Li, and X. Du, "Toward active-site tailoring in heterogeneous catalysis by atomically precise metal nanoclusters with crystallographic structures," *Chem. Rev.*, vol. 121, no. 2, pp. 567–648, 2020.

[8] X. Du *et al.*, "CO2 and CH4 adsorption on different rank coals: A thermodynamics study of surface potential, Gibbs free energy change and entropy loss," *Fuel*, vol. 283, p. 118886, 2021.

[9] T. Yoon, W. Park, J. You, and S. Na, "Investigation of Direct Electron Transfer of Glucose Oxidase on a Graphene-CNT Composite Surface: A Molecular Dynamics Study Based on Electrochemical Experiments," *Nanomaterials*, vol. 14, no. 13, 2024. DOI: https://doi.org/10.3390/nano14131073.

[10] Y. Han, P. Zhang, X. Duan, X. Gao, and L. Gao, "Advances in precise synthesis of metal nanoclusters and their applications in electrochemical biosensing of disease biomarkers," *Nanoscale*, 2025.

[11] E. Hosseinzadeh, A. Foroumadi, and L. Firoozpour, "A DFT study on the transition metal doped BN and AlN nanocages as a drug delivery vehicle for the cladribine drug," *J. Mol. Liq.*, vol. 374, p. 121262, 2023.

[12] K. K. Singh, "A DFT studies on absorbing and sensing possibilities of glucose on graphene surface doped with Ag, Au, Cu, Ni & Pt atoms," *Biosens. Bioelectron. X*, vol. 13, p. 100287, 2023.

[13] A. Saikia, R. Newar, S. Das, A. Singh, D. J. Deuri, and A. Baruah, "Scopes and challenges of microfluidic technology for nanoparticle synthesis, photocatalysis and sensor applications: A comprehensive review," *Chem. Eng. Res. Des.*, vol. 193, pp. 516–539, 2023.

[14] P. K. Chattaraj and D. R. Roy, "Update 1 of: electrophilicity index," *Chem. Rev.*, vol. 107, no. 9, pp. PR46–PR74, 2007.

[15] T. Koopmans, "Über die Zuordnung von Wellenfunktionen und Eigenwerten zu den Einzelnen Elektronen Eines Atoms," *Physica*, vol. 1, no. 1, pp. 104–113, 1934. DOI: https://doi.org/https://doi.org/10.1016/S0031-8914(34)90011-2.

[16] X. Jia, H. Zhang, Z. Zhang, and L. An, "First-principles investigation of vacancy-defected graphene and Mn-doped graphene towards adsorption of H2S," *Superlattices Microstruct.*, vol. 134, no. July, 2019. DOI: https://doi.org/10.1016/j.spmi.2019.106235.

[17] T. Sato and H. Nakai, "Density functional method including weak interactions: Dispersion coefficients based on the local response approximation," *J. Chem. Phys.*, vol. 131, no. 22, 2009.

[18] S. Tomić, B. Montanari, and N. M. Harrison, "The group III–V's semiconductor energy gaps predicted using the B3LYP hybrid functional," *Phys. E Low-dimensional Syst. Nanostructures*, vol. 40, no. 6, pp. 2125–2127, 2008.

[19] A. A. Salari, "Are the inorganic B24N24, Al24N24, B24P24 and Al24P24 nanoclusters synthesizable or not? A DFT study," *Inorganica Chim. Acta*, vol. 456, pp. 18–23, Feb. 2017. DOI: https://doi.org/10.1016/J.ICA.2016.11.006.

[20] A. Wang, J. Cui, L. Zhang, L. Liang, Y. Cao, and Q. Liu, "The chemical recognition of hydrogen fluoride via B24N24 nanocage: quantum chemical approach," *J. Mol. Model.*, vol. 29, no. 12, p. 386, 2023. DOI: https://doi.org/10.1007/s00894-023-05727-w.

[21] A. Frisch, "gaussian 09W Reference," Wallingford, USA, 25p, vol. 470, 2009.

[22] M. Caricato, M. J. Frisch, A. Frisch, J. Hiscocks, and M. J. Frisch, Gaussian 09 IOps reference manual. 2013. [Online]. Available: http://www.gaussian.com/g_tech/g_iops/iops2.pdf

[23] M. García-Valverde, N. A. Cordero, and E. S. de la Cal, "GAUSSVIEW® as a tool for learning organic chemistry," in EDULEARN15 Proceedings, IATED, 2015, pp. 4366–4370.

[24] A. N. D. L. Duality and I. Im, "G A U S S I A N S U M RULES IN Q U A N T U M C H R O M O D Y N A M I C S I ?," vol. 250, pp. 61–108, 1985.

[25] S. Resan, R. Hameed, A. Al-Hilo, and M. Al-Anber, "The impact of torsional angles to tune the nonlinear optical response of

chalcone molecule: Quantum computational study," *Rev. Cuba. Fis.*, vol. 37, no. 2, pp. 95–100, 2020.

[26] M. J. Al-anber, "Theoretical Semi-empirical Study of the Glycine Molecule Interaction with Fullerene C60," *Orbital Electron. J. Chem.* North Americ, 2014, [Online]. Available: http://www.orbital.ufms.br/index.php/Chemistry/article/view/491

[27] H. Xiong, B. Liu, H. Zhang, and J. Qin, "Theoretical insight into two-dimensional M-Pc monolayer as an excellent material for formaldehyde and phosgene sensing," *Appl. Surf. Sci.*, vol. 543, p. 148805, 2021. DOI: https://doi.org/https://doi.org/10.1016/j.apsusc.2020.148805.

[28] R. Xue, C. Wang, Y. Wang, Q. Guo, E. Dai, and Z. Nie, "Metal Embedded Phthalocyanine Monolayers as Promising Materials for Toxic Formaldehyde Gas Detection: Insights from DFT Calculations," *Metals (Basel).*, vol. 12, no. 9, 2022. DOI: https://doi.org/10.3390/met12091442.

[29] Y. Yong, H. Cui, Q. Zhou, X. Su, Y. Kuang, and X. Li, "C2N monolayer as NH3 and NO sensors: A DFT study," *Appl. Surf. Sci.*, vol. 487, pp. 488–495, 2019. DOI: https://doi.org/https://doi.org/10.1016/j.apsusc.2019.05.040.

[30] B. Gergen, H. Nienhaus, W. H. Weinberg, and E. W. McFarland, "Chemically induced electronic excitations at metal surfaces," *Science*, vol. 294, no. 5551, pp. 2521–2523, 2001.

[31] G. Hoffmann, H. Chermette, and C. Morell, "Revisiting nucleophilicity: an index for chemical reactivity from a CDFT approach," *J. Mol. Model.*, vol. 30, no. 7, pp. 0–23, 2024. DOI: https://doi.org/10.1007/s00894-024-06020-0.

[32] I. Torres, S. Mehdi Aghaei, A. Rabiei Baboukani, C. Wang, and S. Bhansali, "Individual Gas Molecules Detection Using Zinc Oxide–Graphene Hybrid Nanosensor: A DFT Study," C, vol. 4, no. 3, p. 44, 2018. DOI: https://doi.org/10.3390/c4030044.

[33] Y. Q. Su *et al.*, "Stability of heterogeneous single-atom catalysts: a scaling law mapping thermodynamics to kinetics," *npj Comput. Mater.*, vol. 6, no. 1, 2020. DOI: https://doi.org/10.1038/s41524-020-00411-6.

[34] B. J. Cid *et al.*, "Metal-decorated siligene as work function type sensor for NH3 detection: A DFT approach," *Appl. Surf. Sci.*, vol. 610, no. October 2022, pp. 1–8, 2023. DOI: https://doi.org/10.1016/j.apsusc.2022.155541.

[35] A. Manuscript *et al.*, "Manuscript version : Accepted Manuscript van der Waals forces in density functional theory : The vdW- DF method".

[36] T. Lenhart, K. Eckhardt, N. Fohrer, and H.-G. Frede, "Comparison of two different approaches of sensitivity analysis," *Phys. Chem. Earth*, Parts A/B/C, vol. 27, no. 9–10, pp. 645–654, 2002.

[37] T. Most and J. Will, "Sensitivity analysis using the Metamodel of Optimal Prognosis," arXiv Prepr. arXiv2408.03590, 2024.

[38] J. Wang, "Electrochemical glucose biosensors," *Chem. Rev.*, vol. 108, no. 2, pp. 814–825, 2008.

[39] M. Shokrekhodaei and S. Quinones, "Review of non-invasive glucose sensing techniques: optical, electrical and breath acetone," *Sensors*, vol. 20, no. 5, p. 1251, 2020.

[40] H. Li *et al.*, "Chemical and biomolecule sensing with organic field-effect transistors," *Chem. Rev.*, vol. 119, no. 1, pp. 3–35, 2018.

[41] A. Panahi *et al.*, "DNA adsorption monitoring with interdigital open-gate junction field effect transistor for DNA storage applications: MD modeling, design, and experimental results," *Sensors Actuators A Phys.*, vol. 381, p. 116076, 2025.

[42] M. M. R. Nayini, H. Sayadian, N. Razavipour, and M. Rezazade, "Chemical-sensing of Amphetamine drug by inorganic AlN nano-cage: A DFT/TDDFT study," *Inorg. Chem. Commun.*, vol. 121, no. July, p. 108237, 2020. DOI: https://doi.org/10.1016/j.inoche.2020.108237.

[43] P. A. Monson, "Understanding adsorption/desorption hysteresis for fluids in mesoporous materials using simple molecular models and classical density functional theory," *Microporous Mesoporous Mater.*, vol. 160, pp. 47–66, 2012.

[44] A. Sharma, M. S. Khan, and M. Husain, "Adsorption of phosgene on Si-embedded MoS 2 sheet and electric field-assisted desorption: insights from DFT calculations," *J. Mater. Sci.*, vol. 54, pp. 11497–11508, 2019.

[45] K. Patel, B. Roondhe, S. D. Dabhi, and P. K. Jha, "A new flatland buddy as toxic gas scavenger: A first principles study," *J. Hazard. Mater.*, vol. 351, pp. 337–345, 2018. DOI: https://doi.org/https://doi.org/10.1016/j.jhazmat.2018.03.006.

Citación del artículo:
R. Hameed and M. Al-Anber, "α-D-Glucose Adsorption on $Al_{24}N_{24}$ and Transition Metal-Doped $Al_{23}N_{24}$ Nanoclusters: New Insights for Biodetection", *Rev. Colomb. Quim.*, vol. 53, no. 2, pp. 19–28, 2024. DOI: https://doi.org/10.15446/rev.colomb.quim.v53n2.118870